AIP | Applied Physics Letters

Non-equilibrium oxidation states of zirconium during early stages of metal oxidation

Wen Ma, F. William Herbert, Sanjaya D. Senanayake, and Bilge Yildiz

Citation: Applied Physics Letters **106**, 101603 (2015); doi: 10.1063/1.4914180
View online: http://dx.doi.org/10.1063/1.4914180
View Table of Contents: http://scitation.aip.org/content/aip/journal/apl/106/10?ver=pdfcov
Published by the AIP Publishing

Non-equilibrium oxidation states of zirconium during early stages of metal oxidation

Wen Ma,[1] F. William Herbert,[1,2] Sanjaya D. Senanayake,[3] and Bilge Yildiz[1,a)]
[1]*Laboratory for Electrochemical Interfaces, Department of Nuclear Science and Engineering, Massachusetts Institute of Technology, 77 Massachusetts Avenue, Cambridge, Massachusetts 02139, USA*
[2]*Department of Materials Science and Engineering, Massachusetts Institute of Technology, 77 Massachusetts Avenue, Cambridge, Massachusetts 02139, USA*
[3]*Chemistry Department, Brookhaven National Laboratory, Upton, New York 11973, USA*

(Received 21 January 2015; accepted 23 February 2015; published online 11 March 2015)

The chemical state of Zr during the initial, self-limiting stage of oxidation on single crystal zirconium (0001), with oxide thickness on the order of 1 nm, was probed by synchrotron x-ray photoelectron spectroscopy. Quantitative analysis of the Zr 3*d* spectrum by the spectrum reconstruction method demonstrated the formation of Zr^{1+}, Zr^{2+}, and Zr^{3+} as non-equilibrium oxidation states, in addition to Zr^{4+} in the stoichiometric ZrO_2. This finding resolves the long-debated question of whether it is possible to form any valence states between Zr^0 and Zr^{4+} at the metal-oxide interface. The presence of local strong electric fields and the minimization of interfacial energy are assessed and demonstrated as mechanisms that can drive the formation of these non-equilibrium valence states of Zr.
 [http://dx.doi.org/10.1063/1.4914180]

Knowing the chemical and structural nature of the initial oxide formed on metal surfaces is important for quantifying the oxidation mechanism and kinetics in corrosion science,[1] as well as for fundamental studies in electrochemistry[2] and catalysis.[3,4] The oxidation of zirconium is of interest for various technologies, including structural materials for nuclear reactors,[5] corrosion-resistant coatings,[5,6] electrolytes for advanced solid oxide fuel cells,[7] redox based resistive switching memory devices,[8] gate dielectric for metal oxide semiconductor devices,[9] and even for bio-implants.[10]

It is well known that oxygen diffuses inwards across the oxide film while cations are relatively immobile during the oxidation of Zr.[11] Therefore, the new oxide layers form at the metal/oxide interface as the oxidation progresses. Oxygen diffusion assisted by an electric field (Mott potential) governs the early stages of metal oxidation.[12–14] The transport kinetics of oxygen through the oxide layer is controlled by the defect chemistry and mobility, and by the electric field strength that depends on the electronic structure of the oxide. Thus, it is important to know the chemical and electronic state of the zirconium oxide to develop accurate oxidation models. However, the chemical state of the early oxide on zirconium has remained elusive for almost three decades due to prior challenges in experimental and analytical approaches. In this work, by combining synchrotron x-ray photoelectron spectroscopy (XPS) measurements and physical modeling of the spectrum, we revealed unequivocally the presence of 1+, 2+, and 3+ as non-equilibrium oxidation states of Zr during the initial stages of oxidation, in addition to the expected 4+ state of the stoichiometric oxide. We have proven the mechanisms for the stabilization of these unexpected lower oxidation states of Zr to be the presence of a strong local electric field during the oxidation process, and the reduction of the interfacial energy between the metal and the oxide.

Unlike the reducible oxides such as TiO_2,[15] SnO_2,[16] and CeO_2[17] (where excess electrons localize at the cation sites or delocalize into the conduction band), the Zr cation in ZrO_2 is energetically very difficult to reduce,[18–20] rendering this material practically irreducible. The charge states of Zr are expected to be either Zr^0 as in the metal or Zr^{4+} as in the stoichiometric oxide ZrO_2. While the oxidation of Zr metal progresses inwards, the incipiently oxidized layer is buried beneath the full oxide that is exposed at the top surface. This inner layer is called the *initial oxide* or the *sub-oxide*.[21] Several studies using different surface analysis techniques suggested the existence of Zr sub-valence states (valence states between Zr^0 and Zr^{+4}) as part of this sub-oxide.[20,22] However, there remains no conclusive proof of the number and nature of the sub-valence states, without a consistency among the reported results. We believe there are three reasons to explain the large discrepancy among results related to Zr sub-valence states characterized by previous XPS studies.[23] First, most of the XPS measurements on Zr 3*d* photoelectron spectrum scanned only the main peak (175 eV–190eV), omitting the intrinsic energy loss contribution arising from the coupling of the core hole with collective electron oscillations at higher binding energies (BEs) (190 eV–210 eV). Neglecting this intrinsic energy loss contribution leads to inaccuracies,[24] because the cross section of intrinsic energy loss is different for Zr metal and for Zr oxide(s). The second possible reason behind the discrepancy is the limitation of instrumental resolution of laboratory XPS equipment used, both in terms of depth and energy, which makes it impossible to resolve any states from the thin sub-oxide buried underneath the full oxide layer (see Sec. VII of supplementary material).[25] Third, the analyses of the Zr 3*d* photoelectron spectra in most of the prior studies were performed by simple peak fitting, using conventional background subtraction and standard peak shapes. This empirical approach

a)Author to whom correspondence should be addressed. Electronic mail: byildiz@mit.edu

is not sufficient to resolve the complicated photoelectron emission peaks of Zr 3*d* which has an intrinsic energy loss. In this work, we employ the "spectrum reconstruction" method of Lyapin and Graat[24,26] to quantitatively analyze our Zr 3*d* photoemission peaks that were measured using high-resolution synchrotron XPS. The essence of the spectrum reconstruction method is the inclusion of models and corrections that are all based on the physical process of photoelectron emission, including the intrinsic energy loss peak. In addition, the soft x-ray radiation from synchrotron sources, with enhanced signal intensity, superior energy resolution, and lower photon energy (400 eV; IMFP = 0.69 nm, as used in this work) enabled high sensitivity to the formation of the initial thin oxide on Zr.

The oxidation experiment was performed on a single crystalline Zr (0001) surface, which was cleaned by cycles of Ar^+ ion sputtering (1.5 kV for 30 min) and ultra-high vacuum (UHV) annealing at 1000 K. Oxide films were grown at 300 K by *in situ* exposure of the Zr(0001) surface to pure oxygen with a total pressure of 2×10^{-8} Torr in an UHV system, and was probed by synchrotron x-ray photoelectron spectroscopy (at Brookhaven National Laboratory, NSLS, beam line U12A). The resulting oxide thickness is on the order of 1 nm in this study. In order to verify the formation of Zr sub-oxide under an electric field, a separate experiment was conducted. Fully oxidized dense ZrO_2 thin films (200 nm thick, monoclinic) were deposited onto $SrTiO_3$ (001) substrates by pulsed laser deposition (PLD). Electric field was applied to these ZrO_2 thin films by using interdigitated Ti(20 nm)/Pt(100 nm) microelectrodes prepared by DC sputtering and photolithographic lift-off.

The evolution of the Zr valence state as a function of increasing oxygen exposure (time) could be captured from the Zr 3*d* spectra (Figure 1). The geometry used in the experiment and in the spectrum reconstruction analysis for the initial oxidation of Zr(0001) is illustrated in Figure 1(a). The x-ray (with photon energy 400 eV) is incident at 30° with respect to sample normal, while the XPS analyzer collects electrons at 35° to the sample normal. The two-layer oxide model is used in the photoelectron spectrum reconstruction; the Zr sub-oxide (ZrO_x) layer is sandwiched between Zr metal on the bottom and ZrO_2 on the top. The Zr 3*d* x-ray photoelectron spectra of pure Zr metal (Zr^0 in Zr metal) and the fully oxidized Zr surface (Zr^{4+} in ZrO_2) are shown in Figure 1(b) as reference, including both the measured data and the reconstructed final spectrum for each (see Sec. I of supplementary material[25] and Refs. 24 and 26 for the modelling of the spectra). A distinctive feature of the spectra is the intrinsic contribution at high binding energy (190 eV–210 eV) originating from the coupling of the core hole with collective electron oscillations.[24] The final reconstructed spectra for Zr^0 and Zr^{4+} states here gave a very good agreement with the experimentally measured spectra. By using these reference spectra, subsequent intermediate oxidation spectra were fitted, as explained in Sec. I of the supplementary material.[25]

Figure 1(c) shows the Zr 3*d* photoelectron peaks for a series of successive O_2 exposures at 300 K and 2×10^{-8} Torr of

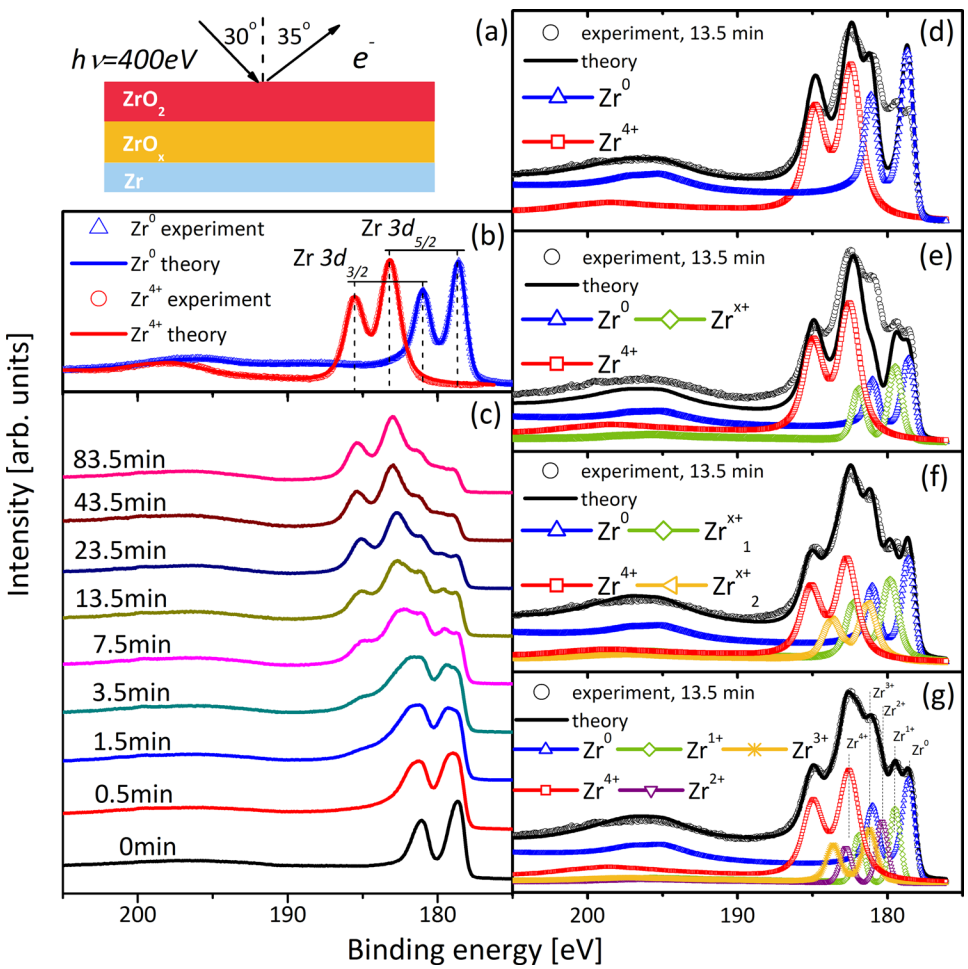

FIG. 1. Zr 3*d* x-ray photoelectron spectra during oxidation of Zr(0001) single crystal in 2×10^{-8} Torr dry oxygen at 300 K, measured with photon energy of 400 eV. (a) Schematic of the geometry used in the XPS experiment and in the spectrum reconstruction analysis for the initial oxidation of Zr(0001). (b) Reference Zr 3*d* spectra for Zr^0 (obtained prior to oxidation) and for Zr^{4+} (obtained after 2 h of oxidation in 2×10^{-6} Torr dry oxygen at 500 K). Solid lines refer to the spectrum reconstruction results for Zr^0 and Zr^{4+}. (c) Consecutive Zr 3*d* spectra from 0 min to 83.5 min of oxygen exposure. (d)–(g) Spectrum reconstruction results for Zr 3*d* spectra taken at 13.5 min of oxidation in 2×10^{-8} Torr dry oxygen at 300 K, with (d) no sub-valence state peaks, (e) one sub-valence state peak, (f) two sub-valence state peaks, (g) three sub-valence state peaks. Zr^{x+} in (e) and (f) denotes the sub-valance that is either 1+, or 2+, or 3+. The sum of squared residuals of the reconstructed normalized spectra with respect to the experimental normalized spectra is 11.8 in (d), 4.2 in (e), 0.4 in (f), and 0.1 in (g) (Error analysis in Sec. I of supplementary material).[25]

oxygen pressure. Prior to oxidation (at time = 0 min), only metallic peaks are visible in the spectra. As the oxidation time is increased to 0.5 min and 1.5 min, the metallic peaks broaden due to the formation of Zr sub-oxide states. After 3.5 min O_2 exposure, the Zr^{4+} peaks become prominent, and continue to increase in signal intensity with further O_2 exposure, indicating the formation of stoichiometric ZrO_2 oxide at the surface. For the oxidation spectra obtained after 3.5 min, 7.5 min, and 13.5 min, intermediate peaks appear, not coinciding either with the Zr^0 or Zr^{4+} peaks, giving a strong evidence for the formation of Zr sub-valence states.

We lend further credence to the existence of Zr sub-oxide through our quantitative analysis of the Zr 3*d* photoelectron spectra from the oxidized samples. Accurate fitting could not be achieved with just the metallic and one oxidic component alone (Figure 1(d)). Instead, several additional doublet peaks corresponding to the Zr sub-valence states had to be added to attain the best fit to the spectra. Between one and three additional sub valence states were successively included in the reconstruction of the spectra, as shown in sequence of Figures 1(e)–1(g). The quality of each fit was compared, based on square residual errors. The best fit reconstructed spectra was obtained by adding three sub-valence states, Zr^{1+}, Zr^{2+}, and Zr^{3+}, peaks between the metallic (Zr^0) and the fully oxidic (Zr^{4+}) peaks (Figure 1(g)). The line shape of the individual sub-valence peaks was assumed to be the same as oxidic (Zr^{4+}) peak. The average BE values of 179.83 ± 0.05 eV, 180.99 ± 0.05 eV, and 182.10 ± 0.05 eV, as determined for the positions of the main Zr 3*d* peak of sub-valence Zr^{1+}, Zr^{2+}, and Zr^{3+} components, are in between the corresponding BE values of the metallic and ZrO_2 main peaks at 178.66 ± 0.05 and 183.25 ± 0.05 eV, respectively. The almost equal spacing of the sub-valence state peaks is in agreement with the fact that the valence charge transfer (ionization energy) and the crystalline field (Madelung energy) contributions to the chemical shift are expected to be approximately proportional to ionicity or oxidation state.[27] Our result on the formation of the Zr^{1+}, Zr^{2+}, and Zr^{3+} components in the sub-oxide is applicable to all the spectra taken at times 0.5 min to 83.5 min as shown in Figure S1.

The fraction and relative intensity of Zr sub-valence states in the total oxide layer was quantified from the spectrum reconstruction. The sub-valence states are formed after less than 2 min of exposure. As the oxide thickens, the fraction of Zr^{4+} (full oxide) increases while the aggregate signal from the sub-valence states drops to a constant level (Figures 2(a) and 2(b)). More interestingly, the sub-oxide persists at a constant thickness at the Zr/ZrO_2 interface for the oxidation times at or longer than 20 min (Figure 2(a)). The average composition within the sub-oxide layer is $ZrO_{1 \pm 0.05}$, which is calculated by taking the average of the fractional contributions of Zr^{1+}, Zr^{2+}, and Zr^{3+} from Figure 2(a), as plotted then in Figure 2(b). It must be noted that the earlier observation of a "ZrO" stoichiometry found by atom probe tomography in the sub-oxide upon oxidation of Zr[21] does not mean that the only oxidation state is 2+ as in ZrO. An average of all Zr^{1+}, Zr^{2+}, and Zr^{3+} can give rise to a ZrO-like composition, while the local chemistry and coordination can be different than ZrO, as found in this work.

At thermodynamic equilibrium[19,28] with the temperatures and oxygen pressure used in our experiments, the 1+, 2+, and 3+ oxidation states of Zr are not expected to exist in the bulk of zirconium oxide. Here we propose two possible drivers for the stabilization of these sub-valence states of oxidation: (i) the strong electric field (Mott potential) present across the oxide layer and (ii) the minimization of the interfacial energy. First, we assess the role of the electric field. Mott potential is treated as a driver to the oxidation kinetics by assisting oxygen migration in the classical Cabrera-Mott model.[12] However, electric field can also couple to the thermodynamics of the oxide as an external energy source, and can drive the formation of intermediate reduced states of Zr during oxidation. By fitting our oxidation kinetics data to the Cabrera-Mott model (Figure 2(d)), the Mott potential was found to be 0.069 V, yielding a very strong electric field (E = 0.6 MV/cm) across the 1.1 nm oxide. The presence of this electric field can change the energy landscape of the metal-oxide interface and lead to the stabilization of the sub-oxide compositions that are far from the equilibrium state. While the formation of a non-equilibrium Zr-oxide composition under electric field was suggested by prior *ab initio*

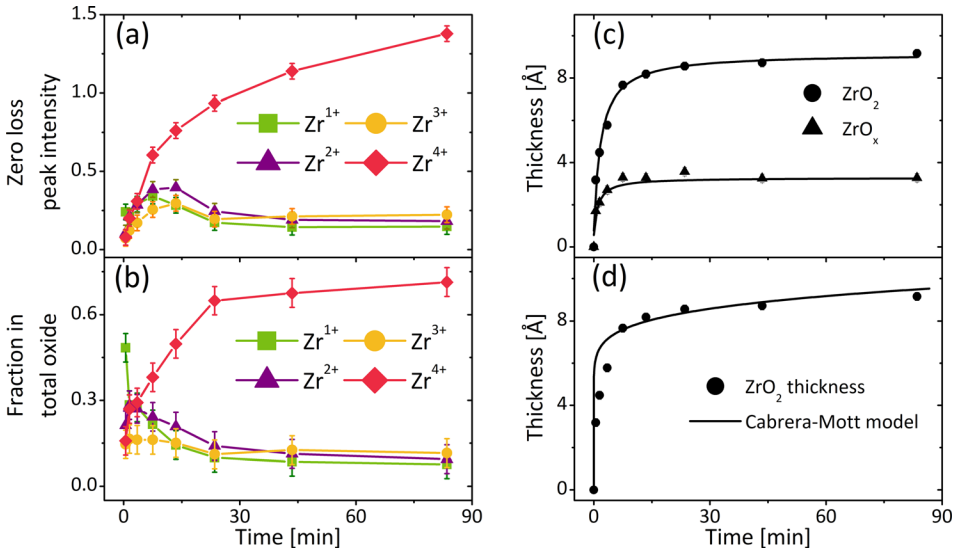

FIG. 2. Chemical states and oxide thicknesses as a function of time during the oxidation of Zr(0001) single crystal in 2×10^{-8} Torr dry oxygen at 300 K. (a) Zero loss peak intensity (from Zr 3*d* photoelectron spectra reconstruction) of Zr^{1+}, Zr^{2+}, Zr^{3+}, and Zr^{4+} (renormalized by zero loss peak intensity of Zr^0). (b) Fraction of of Zr^{1+}, Zr^{2+}, Zr^{3+}, and Zr^{4+} in the total oxide that is given by the sum of Zr^{1+}, Zr^{2+}, Zr^{3+}, and Zr^{4+} in (a). (c) Oxide thickness and sub-oxide thickness as a function of oxidation time. (d) Fitting of the total oxidation kinetics by using the Cabrera-Mott model (see Sec. II of supplementary material[25]).

computations,[29] no prior experiment was able to directly prove the formation of such a sub-stoichiometric Zr-oxide under an electric field. To verify this argument, we applied 10 V of bias laterally on a thin film of the fully oxidized ZrO_2 between the two sets of finger-like electrodes (inset of Figure 3), and measured the evolution of the Zr 3*d* spectrum. The applied bias corresponds to an electric field of 0.005 MV/cm in this geometry; a substantial field magnitude. A clear shoulder was found to evolve at binding energies lower than the Zr^{4+} peaks in the Zr 3*d* spectrum (Figure 3). The position of this new contribution to the spectrum does not match that of Zr^0 peaks, and thus, is not associated with a full reduction of the oxide down to the metallic state. By using the positions of the intermediate oxidation states of Zr that we deduced in Figure 1, we identified that the new composition formed in the ZrO_2 film under electric field include Zr^{3+} and/or Zr^{2+} states. From these results, we can conclude that the even stronger electric field present during the initial oxidation of Zr (0.6 MV/cm here) is a plausible driver to the stabilization of the 1+, 2+, and 3+ states of Zr in the early oxide.

Second, we assess the effect of the interfacial energies by modelling the thermodynamic stability of a thin amorphous sub-oxide layer between the full oxide and the metal. Two scenarios are compared: model (a) has a layer of full oxide (ZrO_2) with thickness h_1 formed directly on single crystal Zr(0001) and model (b) has a sub-oxide (ZrO_x) layer (thickness h_s) sandwiched between the full oxide (ZrO_2 with thickness h_2) and single crystal Zr(0001). The total Gibbs free energy difference between model (a) and model (b), $\Delta G = G_a - G_b$, can be expressed as follows (see Ref. 30 and Sec. IV of supplementary material[25] for details):

$$\Delta G = \frac{h_s}{\Omega_s}\left(\frac{1}{2}G_{ZrO_2} - G_{ZrO_x}\right) + \frac{p}{2A_o}\left(\Delta H^{\infty}_{O\,in\,m} - \Delta H^{\infty}_{O\,in\,ZrO_x}\right), \tag{1}$$

where Ω_s is the molar volume of ZrO_x; G_{ZrO_2} and G_{ZrO_x} are the bulk Gibbs free energy of 1 mol ZrO_2 and ZrO_x, respectively; $\Delta H^{\infty}_{O\,in\,m}$ and $\Delta H^{\infty}_{O\,in\,ZrO_x}$ are the enthalpy of mixing at infinite dilution of 1 mol O atoms in Zr crystalline metal and in ZrO_x, respectively; p is the fraction of total interface area of O atomic cell in contact with Zr metal atom in crystalline metal; A_o is the interfacial area of the cell that contains 1 mol of oxygen atoms.

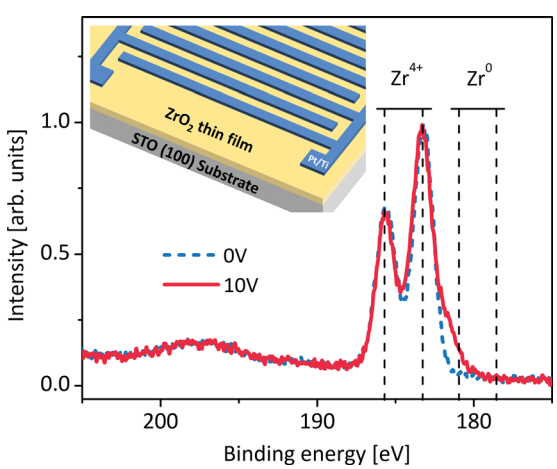

FIG. 3. Zr 3*d* photoelectron spectrum before and after applying 10 V electric bias to the ZrO_2 thin film, corresponding to an average electric field of 0.005 MV/cm between the interdigitated electrodes. The inset shows the schematic drawing of the interdigitated electrode structures used for applying electric field through the PLD-deposited monoclinic ZrO_2 dense film. The sample was kept at 550 K and 1×10^{-10} Torr in both data sets (with 0 V and at/after 10 V).

Values for oxide thicknesses (h_1, h_2, h_s) grown on Zr(0001) were obtained by calculating the attenuation of the metal zero loss peak intensity. Figures 2(c) and 2(d) show the calculated sub-oxide and oxide thicknesses. The free energy of amorphous ZrO_2 is obtained by assuming it to be the same as ZrO_2 liquid: $G_{ZrO_2} = -972.661$ kJ/mol.[31] Since there are no previously reported values of Ω_s, G_{ZrO} and $\Delta H^{\infty}_{O\,in\,ZrO}$ for amorphous ZrO_x sub-oxide, we use the value for crystalline ZrO reported in the literature,[32] as $\Omega_s = 0.0875\,nm^3$, $G_{ZrO} = -539$ kJ/mol, and $\Delta H^{\infty}_{O in ZrO} \cong 1.2 G_{ZrO} + 100 = -547$ kJ/mol. We take $\Delta H^{\infty}_{O in m} = -449$ kJ/mol,[33] $p = \frac{1}{3}$[30], and $A_o = 0.127\,nm^2$. The resulting Gibbs free energy difference between model (a) and model (b) is $\Delta G = G_a - G_b = 3.3\,eV/nm^2$. This analytical estimation based on interface formation energies indicates that a tri-layered structure of $ZrO_2/ZrO_x/Zr$ (as in model (b)) is energetically more stable compared to an abrupt interface between stoichiometric ZrO_2 and crystalline metal Zr.

We believe that the formation of the Zr valence states between 0 and 4+ is a signature of oxide precursor formation on metals that have high solubility of oxygen. For example, the Ti^{2+} and Ti^{3+} were found to form preferentially at the metal/oxide interface during the Ti metal oxidation, where the full oxide is TiO_2.[34] Tantalum also is known to form Ta_2O, TaO and Ta_2O_3 states prior to the fully oxidized state in Ta_2O_5.[13] Similarly one can expect sub-oxide formation during oxidation of Hf, though not yet demonstrated. Interestingly, even metals like Pt[3] and Pd,[35] which are "less active" to oxygen, also form precursor states at the surface prior to full oxidation. The difference of Zr compared to Ti or Ta is that electron localization on the zirconium cation in ZrO_2 is energetically very, very expensive compared to that in TiO_2 or Ta_2O_5 (for example, as a local metric, a neutral oxygen vacancy formation energy in ZrO_2 is 7.2 eV compared to 4 eV in TiO_2[20]). This literally irreducible nature of ZrO_2 under any practical condition has made it more difficult to observe the intermediate oxidic components clearly and systematically prior to our work.

The Zr sub-oxide states identified in this work could also reveal the mechanism for the red-ox based resistive switching in memory devices made of ZrO_2. Indeed, there is evidence from experiments[36] and computational simulations[29] that lower-resistance states (with higher electronic conductivity) in such devices are due to the formation of sub-stoichiometric oxides. However, no direct *in situ* observation of such sub-oxide states under electric field has been achieved before for ZrO_2. The finding of Zr^{2+} and Zr^{3+} after applying an electric field on fully oxidized ZrO_2 films could provide the chemical states responsible for the resistive switching observed in this material. This is a realization of the electric field modulation of oxygen defects in oxides, whose importance is being realized more recently for oxide-based electronic and electrochemical devices.[37]

In summary, we uncover the non-equilibrium valence states of Zr during the early stage oxidation of the metal in oxygen gas, probed by high resolution synchrotron x-ray photoelectron spectroscopy and analyzed by physical modeling of the spectrum. Although the average composition yields a stoichiometry of ZrO, as also observed by previous atom probe tomography measurements,[21] the local chemical environments in such a sub-oxide deviate from only the 2+ oxidation state of Zr and include all three Zr^{1+}, Zr^{2+}, and Zr^{3+} states. The mechanisms that drive the formation of Zr sub-oxides at the metal/oxide interface under these experimental conditions have been verified to be: (1) the presence of a strong electric field that changes the energy landscape and modulates the red-ox processes in the oxide and (2) the minimization of the interfacial energy by forming a sub-oxide at the metal-oxide interface. Revealing the presence of such sub-oxides is critical for enabling more accurate oxidation models, as well as for assessing the switching mechanisms and kinetics in red-ox based resistive switching memories.

We gratefully acknowledge the Laboratory Directed Research and Development program (LDRD Project No. 12-026) from Idaho National Laboratory for financial support. The XPS measurements in this work were performed at the National Synchrotron Light Source, a DOE Office of Science User Facility and Brookhaven National Laboratory, supported by the U.S. Department of Energy, Office of Science, Office of Basic Energy Sciences under Contract No. DE-AC02-98CH10886. We thank M. Youssef for useful discussions on the irreducibility of and point defects in ZrO_2. We thank D. Mullins and P. Albercht at Oak Ridge National Laboratory for the use of the U12a beamline (Brookhaven National Laboratory) for XPS measurements. We thank J. Anibal Boscoboinik at Brookhaven National Laboratory for help with XPS measurements, and Kurt Broderick at Microsystems Technology Laboratories at MIT for help with sample preparation.

[1]G. S. Was, P. Ampornrat, G. Gupta, S. Teysseyre, E. A. West, T. R. Allen, K. Sridharan, L. Tan, Y. Chen, X. Ren, and C. Pister, J. Nucl. Mater. **371**(1–3), 176 (2007); A. Yilmazbayhan, A. T. Motta, R. J. Comstock, G. P. Sabol, B. Lai, and Z. H. Cai, *ibid.* **324**(1), 6 (2004); K. Xiao, D. Lee, and J. J. Vlassak, Appl. Phys. Lett. **105**(17), 171901 (2014).
[2]I. Popova, V. Zhukov, and J. T. Yates, Phys. Rev. Lett. **89**(27), 276101 (2002); S. K. R. S. Sankaranarayanan, E. Kaxiras, and S. Ramanathan, *ibid.* **102**(9), 095504 (2009); S. Lee, T. L. Meyer, S. Park, T. Egami, and H. N. Lee, Appl. Phys. Lett. **105**(22), 223515 (2014).
[3]D. J. Miller, H. Oberg, S. Kaya, H. S. Casalongue, D. Friebel, T. Anniyev, H. Ogasawara, H. Bluhm, L. G. M. Pettersson, and A. Nilsson, Phys. Rev. Lett. **107**(19), 195502 (2011).
[4]S. Blomberg, M. J. Hoffmann, J. Gustafson, N. M. Martin, V. R. Fernandes, A. Borg, Z. Liu, R. Chang, S. Matera, K. Reuter, and E. Lundgren, Phys. Rev. Lett. **110**(11), 117601 (2013); L. Luo, Y. Kang, J. C. Yang, D. Su, E. A. Stach, and G. Zhou, Appl. Phys. Lett. **104**(12), 121601 (2014).
[5]B. Cox, J. Nucl. Mater. **336**(2–3), 331 (2005).
[6]B. Li, A. R. Allnatt, C. S. Zhang, and P. R. Norton, Surf. Sci. **330**(3), 276 (1995).
[7]N. Q. Minh, J. Am. Ceram. Soc. **76**(3), 563 (1993).
[8]M. Gutowski, J. E. Jaffe, C.-L. Liu, M. Stoker, R. I. Hegde, R. S. Rai, and P. J. Tobin, Appl. Phys. Lett. **80**(11), 1897 (2002).
[9]A. L. Shluger, A. Foster, J. L. Gavartin, and P. V. Sushko, in *Nano and Giga Challenges in Microelectronics*, edited by J. Greer, A. Korkin, and J. Labanowski (Elsevier, Amsterdam, 2003); S. Ramanathan, G. D. Wilk, D. A. Muller, C.-M. Park, and P. C. McIntyre, Appl. Phys. Lett. **79**(16), 2621 (2001); J. Wang, P. P. Freitas, E. Snoeck, P. Wei, and J. C. Soares, *ibid.* **79**(26), 4387 (2001).
[10]B. Cales, Clin. Orthopaed. Relat. Res. **379**, 94 (2000).
[11]G. Bakradze, L. P. H. Jeurgens, T. Acarturk, U. Starke, and E. J. Mittemeijer, Acta Mater. **59**(20), 7498 (2011); M. Yamamoto, C. T. Chan, K. M. Ho, and S. Naito, Phys. Rev. B **54**(19), 14111 (1996).
[12]N. Cabrera and N. F. Mott, Rep. Prog. Phys. **12**, 163 (1949).
[13]F. M. Jacobsen, S. Raaen, M. W. Ruckman, and M. Strongin, Phys. Rev. B **52**(15), 11339 (1995).
[14]N. Cai, G. Zhou, K. Müller, and D. E. Starr, Phys. Rev. B **84**(12), 125445 (2011); N. Cai, G. W. Zhou, K. Muller, and D. E. Starr, Phys. Rev. Lett. **107**(3), 035502 (2011); J. D. Baran, H. Grönbeck, and A. Hellman, *ibid.* **112**(14), 146103 (2014).
[15]U. Diebold, Surf. Sci. Rep. **48**(5–8), 53 (2003).
[16]M. Batzill and U. Diebold, Prog. Surf. Sci. **79**(2–4), 47 (2005).
[17]Z. A. Feng, F. El Gabaly, X. Ye, Z.-X. Shen, and W. C. Chueh, Nat. Commun. **5**, 4374 (2014); F. Esch, S. Fabris, L. Zhou, T. Montini, C. Africh, P. Fornasiero, G. Comelli, and R. Rosei, Science **309**(5735), 752 (2005).
[18]A. S. Foster, V. B. Sulimov, F. L. Gejo, A. L. Shluger, and R. M. Nieminen, Phys. Rev. B **64**(22), 224108 (2001).
[19]M. Youssef and B. Yildiz, Phys. Rev. B **86**(14), 144109 (2012).
[20]C. Gionco, M. C. Paganini, E. Giamello, R. Burgess, C. Di Valentin, and G. Pacchioni, Chem. Mater. **25**(11), 2243 (2013).
[21]Y. Dong, A. T. Motta, and E. A. Marquis, J. Nucl. Mater. **442**(1–3), 270 (2013).
[22]C. Morant, J. M. Sanz, L. Galan, L. Soriano, and F. Rueda, Surf. Sci. **218**(2–3), 331 (1989); P. Sen, D. D. Sarma, R. C. Budhani, K. L. Chopra, and C. N. R. Rao, J. Phys. F-Met. Phys. **14**(2), 565 (1984).
[23]Y. Nishino, A. R. Krauss, Y. P. Lin, and D. M. Gruen, J. Nucl. Mater. **228**(3), 346 (1996); F. Schonbohm, C. R. Fluchter, D. Weier, T. Luhr, U. Berges, S. Doring, and C. Westphal, Phys. Rev. B **80**(16), 165323 (2009); A. Lyapin, L. P. H. Jeurgens, P. C. J. Graat, and E. J. Mittemeijer, J. Appl. Phys. **96**(12), 7126 (2004); C. O. Degonzalez and E. A. Garcia, Surf. Sci. **193**(3), 305 (1988).
[24]A. Lyapin and P. C. J. Graat, Surf. Sci. **552**(1–3), 160 (2004).
[25]See supplementary material at http://dx.doi.org/10.1063/1.4914180 for x-ray photoelectron spectrum analysis, kinetic modeling of Zr oxidation, thermodynamic calculation of interfacial energy, and experimental setup details.
[26]M. Kurth and P. C. J. Graat, Surf. Interface Anal. **34**(1), 220 (2002).
[27]G. D. Mahan, Phys. Rev. B **21**(10), 4791 (1980).
[28]R. W. Vest and N. M. Tallan, J. Am. Ceram. Soc. **48**(9), 472 (1965); L. A. McClaine and C. P. Coppel, J. Electrochem. Soc. **113**(1), 80 (1966).
[29]K.-H. Xue, P. Blaise, L. R. C. Fonseca, and Y. Nishi, Phys. Rev. Lett. **110**(6), 065502 (2013).
[30]L. P. H. Jeurgens, W. G. Sloof, F. D. Tichelaar, and E. J. Mittemeijer, Phys. Rev. B **62**(7), 4707 (2000).
[31]See http://kinetics.nist.gov/janaf/ for thermodynamic parameters for ZrO_2.
[32]B. Puchala and A. Van der Ven, Phys. Rev. B **88**(9), 094108 (2013).
[33]W. E. Wang and D. R. Olander, J. Am. Ceram. Soc. **76**(5), 1242 (1993).
[34]G. Lu, S. L. Bernasek, and J. Schwartz, Surf. Sci. **458**(1–3), 80 (2000).
[35]E. Lundgren, G. Kresse, C. Klein, M. Borg, J. N. Andersen, M. De Santis, Y. Gauthier, C. Konvicka, M. Schmid, and P. Varga, Phys. Rev. Lett. **88**(24), 246103 (2002).
[36]D. Lee, H. Choi, H. Sim, D. Choi, H. Hwang, M. J. Lee, S. A. Seo, and I. K. Yoo, IEEE Electron Device Lett. **26**(10), 719 (2005); J. J. Yang, M. D. Pickett, X. M. Li, D. A. A. Ohlberg, D. R. Stewart, and R. S. Williams, Nat. Nanotechnol. **3**(7), 429 (2008).
[37]S. V. Kalinin and N. A. Spaldin, Science **341**(6148), 858 (2013); S. U. Sharath, T. Bertaud, J. Kurian, E. Hildebrandt, C. Walczyk, P. Calka, P. Zaumseil, M. Sowinska, D. Walczyk, A. Gloskovskii, T. Schroeder, and L. Alff, Appl. Phys. Lett. **104**(6), 063502 (2014).